Bulletin of Mathematical Biology (2002) **64**, 829–860
doi:10.1006/bulm.2002.0303
Available online at http://www.idealibrary.com on IDEAL®

A Two-Variable Model of Somatic–Dendritic Interactions in a Bursting Neuron

CARLO R. LAING* AND ANDRÉ LONGTIN
Department of Physics,
University of Ottawa,
150 Louis Pasteur,
Ottawa, ON,
Canada, K1N 6N5
E-mail: claing@science.uottawa.ca

We present a two-variable delay-differential-equation model of a pyramidal cell from the electrosensory lateral line lobe of a weakly electric fish that is capable of burst discharge. It is a simplification of a six-dimensional ordinary differential equation model for such a cell whose bifurcation structure has been analyzed (Doiron *et al*., *J. Comput. Neurosci.*, **12**, 2002). We have modeled the effects of back-propagating action potentials by a delay, and use an integrate-and-fire mechanism for action potential generation. The simplicity of the model presented here allows one to explicitly derive a two-dimensional map for successive interspike intervals, and to analytically investigate the effects of time-dependent forcing on such a model neuron. Some of the effects discussed include 'burst excitability', the creation of resonance tongues under periodic forcing, and stochastic resonance. We also investigate the effects of changing the parameters of the model.

1. INTRODUCTION

Bursting, in which a cell periodically switches from quiescent behavior to a rapidly spiking state and back again, is an important and common form of behavior (Lisman, 1997; de Vries, 1998; Keener and Sneyd, 1998; Rinzel and Ermentrout, 1998; Izhikevich, 2000; Lemon and Turner, 2000). A number of mathematical models of bursting cells have been developed (Av-Ron *et al*., 1993; Wang, 1993; Sivan *et al*., 1995; de Vries, 1998; Rinzel and Ermentrout, 1998; Doiron *et al*., 2002), but they are generally difficult to treat analytically in any detail. Much past analysis of bursting cells has been influenced by the 'slow–fast' separation of time-scales in bursting systems (Rinzel and Ermentrout, 1998; Izhikevich, 2000), where it is assumed that fast, spiking variables act on a much shorter time-scale than the slow variable(s) that are responsible for the shifts between spiking and quiescent behavior.

* Author to whom correspondence should be addressed.

0092-8240/02/050829 + 32 $35.00/0

Recently, a new mechanism for burst discharge in pyramidal cells of the weakly electric fish *Apteronotus leptorhynchus* was investigated (Doiron *et al*., 2002). These cells receive input directly from electroreceptor cells on the fish's skin, and are thought to play a significant role in the processing of electrosensory information. The model presented in Doiron *et al*. (2002) was a set of six coupled nonlinear first-order ordinary differential equations, which was a reduction from the multicompartment model involving over 1500 variables presented in Doiron *et al*. (2001a). This reduction was obtained by lumping the many compartments into two, representing the soma and the dendrite, and by ignoring the dynamics of the channels not thought to be important in the mechanism for bursting. That the model in Doiron *et al*. (2002) reproduced both the bursting behavior observed in the model of Doiron *et al*. (2001a) and experimentally observed bursts (Lemon and Turner, 2000) indicates that this process was successful.

The model analyzed in Doiron *et al*. (2002) was studied using the 'slow–fast' approach of others (Rinzel and Ermentrout, 1998; Izhikevich, 2000), but it differed from all previous bursting models in that when the one slow variable was held constant, the remaining 'fast' system did not show bistability for any values of the slow variable. The bifurcation in the fast system that ended a burst was found to be a transition from period-one to period-two behavior associated with the failure of a somatic action potential to induce a dendritic one, and the interburst interval was found to involve the passage in phase space near a fixed point. Several aspects of the timing of bursts were found to be related to the distance in parameter space from a saddle–node bifurcation, hence the name 'ghostbursting' (Strogatz, 1994).

In this paper we further reduce the model in Doiron *et al*. (2002) to a set of two discontinuous delay differential equations, from which a two-dimensional map can be derived (assuming constant input current). This gives us analytical insight into complex soma–dendrite interactions, and is computationally much easier to study than an ODE model. The reduced model presented here can be constructed because, as a result of the work in Doiron *et al*. (2002), we understand the essential ingredients of this type of bursting (refer to Fig. 1). A short time after most somatic spikes, current flows from the dendrite to the soma, producing a depolarizing afterpotential (DAP) at the soma. For large enough current injected to the soma, the sizes of these DAPs slowly increase due to a slow inactivation of the dendritic potassium that is responsible for the repolarization of dendritic action potentials. This results in progressively smaller inter-spike intervals (ISIs), and this process continues until an ISI is smaller than the refractory period of the dendrite. Once this happens, there is dendritic spike failure, which removes the normal current flow to the soma, and a DAP does not appear. This results in a long ISI, during which the variable controlling inactivation of dendritic potassium increases, and the sequence starts again. In Fig. 1 we show typical bursting behavior from the model in Doiron *et al*. (2002). The spike patterning is similar to that seen in the multicompartment model in Doiron *et al*. (2001a) and in experimental recordings (Lemon and Turner, 2000).

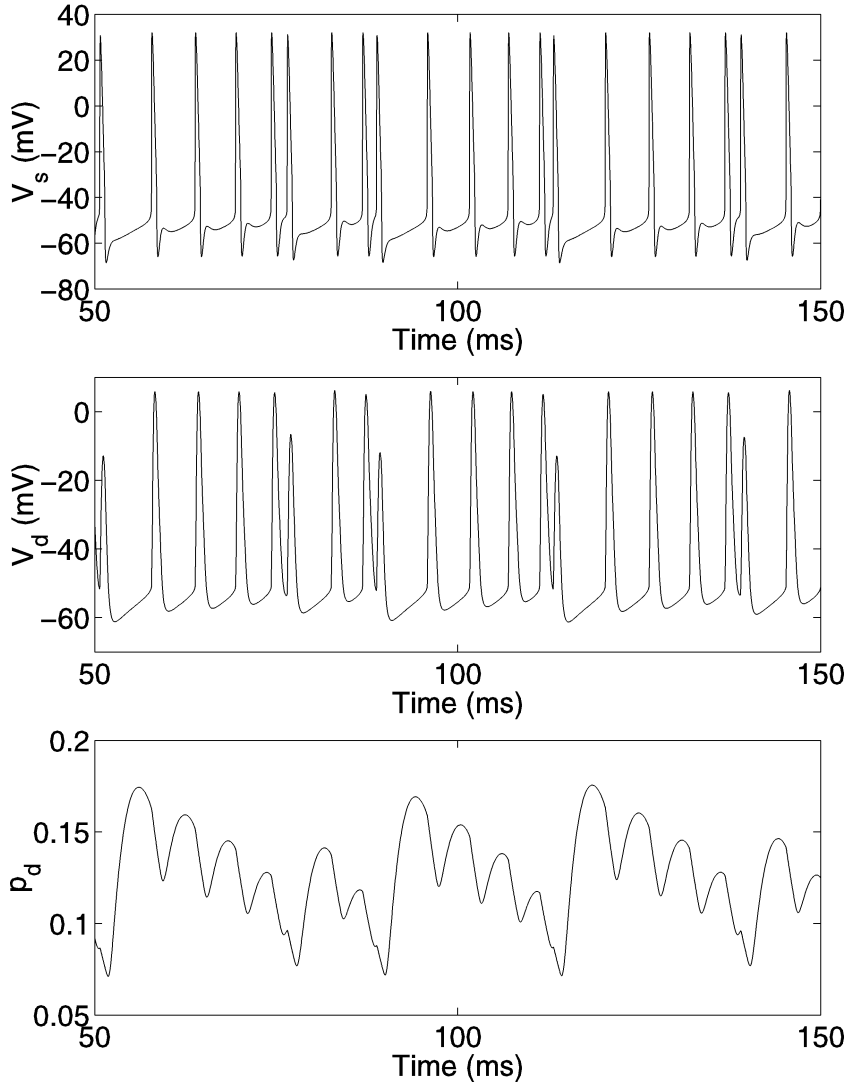

Figure 1. An example of bursting for the 6-variable ODE model of Doiron *et al*. (2002). Top: somatic voltage, middle: dendritic voltage, bottom: dendritic potassium inactivation. Bursts terminate at t approximately 75, 90, 115 and 140. Note the progressively smaller ISIs during a burst, and the dendritic spike failure at the end of each burst.

If we consider gradually increasing the DC current injected into the soma of such an actual pyramidal cell, it is observed that the cell's behavior changes from quiescent to periodic firing and then to bursting (Lemon and Turner, 2000; Doiron *et al*., 2001b). This behavior is also seen in the pyramidal cell models (Doiron *et al*., 2001a, 2002) and the model presented later, and is in marked contrast with many other burst mechanisms for which a cell follows the pattern quiescence, bursting, tonic, as the current is increased (Terman, 1992; Pinsky and Rinzel, 1994; Rinzel and Ermentrout, 1998; Steriade *et al*., 1998).

In this paper we also consider periodically modulating the current applied to the model neuron, and for the case of sinusoidal modulation we obtain a three-dimensional map for successive spike times. This map can be used to determine the boundaries in parameter space of resonance tongues, in which the neuron's firing frequency is locked to that of the forcing. This map is able to explain some of the behavior seen in Laing (2002), in which bursting models [including the one in Doiron *et al*. (2002)] are periodically forced. For example, when only a DC current is injected into the model neuron of Doiron *et al*. (2002), there is a value of current at which the neuron switches from tonic to bursting behavior. However, adding a sinusoidal modulation to the injected current can either increase or decrease the DC value of the current where the transition occurs. The amount of increase or decrease depends on the frequency of the modulation. The simplified model presented here can also reproduce the phenomenon of 'burst excitability' that is explored in more detail in Laing *et al*. (2002b), and by varying parameters, the 'gallery' of burst types seen in Doiron *et al*. (2002).

The two-dimensional model that we have developed would be very useful for large-scale simulations of networks of such neurons as it has fewer variables than common neuron models that involve ionic channels (Doiron *et al*., 2002), the differential equations involved are not stiff, and its piecewise linear nature aids its analysis. The way we have modeled backpropagation of an action potential along a dendrite and the resulting 'ping–pong' effect (Wang, 1999) by a discrete delay in a low-dimensional system is also novel. (The ping–pong effect refers to the interplay between somatic and dendritic action potentials and the electrotonic currents that flow as a result of them not occurring at the same time, nor being of the same duration.) There has been a great deal of recent interest in backpropagation in active dendrites (Segev and Rall, 1998; Häusser *et al*., 2000; Vetter *et al*., 2001), in relation to the processing of synaptic inputs and the induction of synaptic plasticity (Johnston *et al*., 1996). The modeling of active dendrites presented here could possibly be applied to these systems in which backpropagation in active dendrites [or the presence of a second compartment in a two-compartment model (Pinsky and Rinzel, 1994; Mainen and Sejnowski, 1996; Kepecs and Wang, 2000; Booth and Bose, 2001)] is important, provided that the effects of the dendrite on the firing pattern of the soma are understood.

In Section 2 we present the model, derive the corresponding map and investigate its properties, including the effects of changing its parameters. In Section 3 we present the sinusoidally forced model, derive the corresponding map, and discuss resonance tongues and stochastic resonance. Section 4 is a summary and discussion. The appendix contains a discussion of other possible models that show 'ghostbursting'. The point of this is to show that there is not one unique model of this type of behavior, but rather a variety, each of which has its own advantages and disadvantages.

2. THE MODEL

We use an integrate-and-fire neuron (Keener *et al*., 1981) to produce somatic action potentials ('spikes'), and couple this with another variable, c, whose behavior mimics the effects of inactivation of dendritic potassium in the model of Doiron *et al*. (2002) [although c increases during a burst, while the actual inactivation gating variable decreases in Doiron *et al*. (2002) (see Fig. 1); both trends have the same effect in their respective models]. The effective delay between a somatic spike and the appearance of a DAP [a result of the diffusive coupling in voltage between soma and dendrite in Doiron *et al*. (2002)] is mimicked by an actual delay, and the effect of the DAP is mimicked by an instantaneous increase in the neuron's voltage.

The equations are

$$\frac{dV}{dt} = I - V + Ac \sum_n H(t_n - t_{n-1} - r)\delta(t - t_n - \sigma) \tag{1}$$

$$\frac{dc}{dt} = -c/\tau + (B + Cc^2) \sum_n \delta(t - t_n) \tag{2}$$

with the rule $V(t_n^+) = 0$ if $V(t_n^-) = 1$, and the t_n are the times at which the reset occurs (n is an integer). V represents the somatic membrane potential, I is the current injected to the soma, $H(\cdot)$ is the Heaviside function, r represents the refractory period of the dendrite, σ is the effective delay between the somatic action potential and the dendritic-to-somatic current that causes the DAP, and A, B, C and τ are constants. The action potentials are thought of as occurring at the times t_n.

At almost all times, V exponentially approaches I from below with time-constant 1, and c exponentially decays towards 0 with time-constant τ. At each firing time t_n, c is incremented: $c \mapsto c + B + Cc^2$. At a time σ after firing, and assuming that the previous ISI, $t_n - t_{n-1}$, is greater than the refractory period r, V is incremented: $V \mapsto V + Ac$, where c is evaluated at a time σ after firing. If the previous ISI is less than the refractory period, V is not incremented. Note that the neuron will not fire if I is always less than 1.

An example of the behavior of (1), (2) is shown in Fig. 2. Note the increase in the overall level of c and the decrease of ISIs during the burst, and the long ISI separating bursts. This long ISI is a result of the previous ISI being less than the refractory period of the dendrite of the neuron, so that no current propagates from the dendrite to the soma during this ISI. This long ISI can also be seen as the smallest instantaneous frequency in Fig. 3 for I greater than $\sim$1.22. This bursting behavior is quite robust with respect to changes in parameters.

The model (1), (2) has not been formally derived from any other model, but have been constructed as a result of understanding the ionic mechanisms behind ghost-bursting (Doiron *et al*., 2001a, 2002). As mentioned in the appendix, a number of equally valid models could be used. It may be possible to construct similar

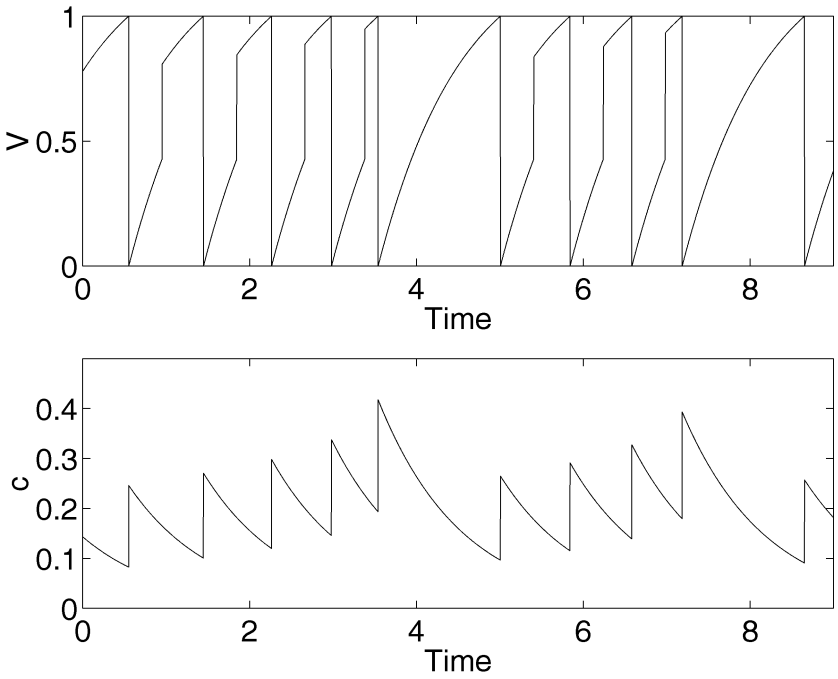

Figure 2. Voltage (top) and c (bottom), the variable representing the amount of feedback from the dendrite to the soma, as functions of time, illustrating the bursting behavior of (1), (2). Parameters are $I = 1.3$, $A = 2.3$, $B = 0.15$, $C = 2$, $r = 0.7$, $\sigma = 0.4$, $\tau = 1$.

models for other types of neurons, provided the interactions between the soma and dendrites are understood.

We now derive an exact map describing the behavior of (1), (2).

2.1. ***Derivation of the map.*** Because of the linearity of (1), (2) for values of t at which the δ functions are zero, it is possible to derive a map for ISIs and values of c just after firing. Recall that the solution of (1) when $A = 0$ is

$$V(t) = I + [V(0) - I]e^{-t}. \tag{3}$$

Assume that $t = t_n^+$, $V(t_n^+) = 0$, $c(t_n^+) = c_n$, and $t_n - t_{n-1} > r$. [$V(t_n^+)$ is defined as $\lim_{\varepsilon \to 0} V(t_n + \varepsilon)$, where $\varepsilon > 0$.] At a time σ after t_n^+, when $V = I(1 - e^{-\sigma})$ and $c = c_n e^{-\sigma/\tau}$, V is incremented by $Ac_n e^{-\sigma/\tau}$. Assuming that this does not push V above 1, i.e., that $I(1 - e^{-\sigma}) + Ac_n e^{-\sigma/\tau} < 1$, V continues to evolve, reaching 1 after a further time s, where

$$I + [I(1 - e^{-\sigma}) + Ac_n e^{-\sigma/\tau} - I]e^{-s} = 1 \tag{4}$$

($s = 0$ when $t = t_n + \sigma$). Solving (4) for s we obtain

$$s = \ln\left(\frac{Ac_n e^{-\sigma/\tau} - Ie^{-\sigma}}{1 - I}\right). \tag{5}$$

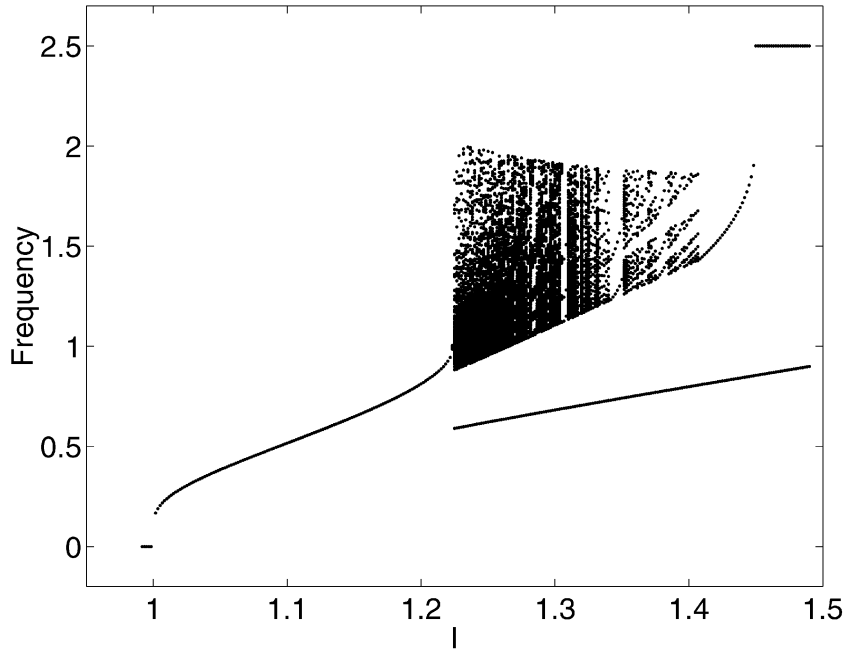

Figure 3. Instantaneous frequency (reciprocal of ISI) as a function of input current, I, for the map (7), (8) (transients have been removed). There is a saddle–node bifurcation of periodic orbits at $I \approx 1.22$. For I greater than $\sim$1.41 the system alternates between a short ISI and a long ISI. Parameters are $A = 2.3$, $B = 0.15$, $C = 2$, $r = 0.7$, $\sigma = 0.4$, $\tau = 1$.

Alternatively, if $t_n - t_{n-1} < r$ (i.e., the last ISI was less than the refractory period of the dendrite, so there is no feedback from dendrite to soma), V will reach 1 after a time

$$\ln\left(\frac{I}{I-1}\right), \tag{6}$$

measured from t_n. During the interval (t_n, t_{n+1}), c exponentially decays with time constant τ, and is then updated at time t_{n+1}. Thus, taking all possible cases into consideration, we have a piecewise two-dimensional map for $\Delta_{n+1} \equiv t_{n+1} - t_n$ and c_{n+1} in terms of Δ_n and c_n:

$$\Delta_{n+1} = \begin{cases} \sigma & \text{if } \Delta_n > r \text{ and } I(1-e^{-\sigma}) + Ac_n e^{-\sigma/\tau} > 1 \quad (i) \\ \sigma + \ln\left(\frac{Ac_n e^{-\sigma/\tau} - Ie^{-\sigma}}{1-I}\right) & \text{if } \Delta_n > r \text{ and } I(1-e^{-\sigma}) + Ac_n e^{-\sigma/\tau} < 1 \quad (ii) \\ \ln\left(\frac{I}{I-1}\right) & \text{if } \Delta_n < r \quad (iii) \end{cases} \tag{7}$$

$$c_{n+1} = c_n e^{-\Delta_{n+1}/\tau} + B + C[c_n e^{-\Delta_{n+1}/\tau}]^2. \tag{8}$$

This is all under the assumption that $I(1 - e^{-\sigma}) < 1$, i.e., that neither I nor σ are too large. If this inequality is not satisfied, e.g., if I is too large, then $\Delta_{n+1} = \ln[I/(I-1)]$ as in case (iii) above. As can be seen from (8), the small value of

Δ_{n+1} in this situation may cause the values of c_i to increase without bound, an unphysical situation. Note that we must have $\sigma < r$.

The instantaneous frequency, i.e., $1/\Delta_n$, is shown as a function of I in Fig. 3 for a particular set of parameter values (transients have been removed). A number of observations can be made:

1. During periodic firing for $1 < I <\sim 1.22$, case (ii) in (7) will always be true. For periodic firing, $c_{n+1} = c_n$, and thus (8) is a quadratic in c_n. It can therefore be solved for c_n in terms of the steady-state period, Δ (the negative square root must be chosen). Substituting this into case (ii) in (7), we obtain an equation that Δ must satisfy:

$$(1-I)e^{-\sigma}e^{\Delta} = \frac{Ae^{-\sigma/\tau}\left[1-e^{-\Delta/\tau}-\sqrt{1-2e^{-\Delta/\tau}+(1-4BC)e^{-2\Delta/\tau}}\right]}{2Ce^{-2\Delta/\tau}} - Ie^{-\sigma}. \tag{9}$$

   For $1 < I <\sim 1.22$, equation (9) has two solutions, the larger one of which is stable (and can be seen in Fig. 3; the unstable solution is not shown). The two solutions coalesce in a saddle–node bifurcation (Kuznetsov, 1995) at $I \sim 1.22$. Note that in (1), (2), this is a saddle–node bifurcation of periodic orbits. Interestingly, it was a saddle–node bifurcation of periodic orbits that separated periodic from bursting behavior in the full ionic ODE model in Doiron *et al*. (2002). As $I \to 1$ from above, the largest root of (9) tends to ∞, corresponding to the frequency tending to zero. Note that if $\tau = 1$, (9) is independent of σ.
2. For I greater than $\sim$1.22, the smallest instantaneous frequency occurs between bursts, where the only current driving the neuron during its entire period is I. Thus the lower curve in Fig. 3 for I greater than $\sim$1.22 is just $\Delta = \ln[I/(I-1)]$ [case (iii) in (7)].
3. For I greater than $\sim$1.22, the 'band' of frequencies in Fig. 3 not including the interburst interval is bounded below by the curve

$$\Delta = \sigma + \ln\left(\frac{ABe^{-\sigma/\tau} - Ie^{-\sigma}}{1-I}\right) \tag{10}$$

   since c_n has a minimum value of B after being reset at the end of the interburst interval. [Expression (10) is obtained by setting $c_n = B$ in (7) (ii).]
4. For I greater than $\sim$1.45, the map alternates between cases (i) and (iii) in (7), so only the longest Δ_n is a function of I. Note that for I greater than $\sim$1.41 the system alternates between a long ISI and a short ISI, which can be thought of as periodically firing 'doublets'.
5. The progression quiescence $\to$ periodic firing $\to$ bursting $\to$ alternating short and long ISIs as I is increased as seen in Fig. 3 is also seen in the models of Doiron *et al*. (2001a, 2002), and experimental recordings (Lemon and Turner, 2000; Turner, 2002).

In relation to point 1 earlier, if the positive square root is taken instead and substituted into case (ii) in (7), the roots of the resulting function may not satisfy the condition $\Delta > r$ associated with case (ii), and thus they will not be actual fixed points of the map. Also, the fact that (8) can be solved explicitly for the steady-state value of c is a result of our choice of the dynamics of c, (2). Replacing the term Cc^2 in (2) by Cc would mean that the equation for the steady state of c was linear and thus had only one solution; this choice would also simplify the expression (9), but would make chaotic behavior more difficult, although not impossible, to obtain (see later).

2.2. ***Lyapunov exponent.*** The Lyapunov exponents of a trajectory determine its stability and the behavior of nearby trajectories. If a stable solution has at least one positive Lyapunov exponent, the system will exhibit sensitivity to initial conditions, and nearby trajectories will typically separate exponentially in time (Drazin, 1992). For a range of current values, the bursting behavior in Doiron *et al*. (2002) was shown to have a positive Lyapunov exponent, and thus be chaotic.

To find the maximal Lyapunov exponent, λ, for a trajectory of the map (7), (8), we analytically calculate the Jacobian, Df, of (7), (8) and evaluate it at each point on the orbit, $x_1, x_2, \ldots$, where $x_i = (\Delta_i, c_i) \in \mathbf{R}^2$. If q_i is the largest magnitude eigenvalue of $Df(x_i)$ then λ can be calculated (Drazin, 1992) from

$$\lambda = \lim_{n\to\infty} \frac{1}{n} \sum_{i=1}^{n} \ln |q_i|. \tag{11}$$

This quantity is shown in Fig. 4, multiplied by four for clarity, together with instantaneous frequency. Note the transition from period-1 firing to chaotic bursting at $I \sim 1.22$, and the long-period quasiperiodic behavior for I greater than $\sim$1.32.

2.3. ***Effects of parameters.*** The model (1), (2) has six parameters that are regarded as constant (A, r, σ, τ, B and C). We now briefly discuss the effects of changing each of these. In more realistic models (Doiron *et al*., 2001a, 2002), changing parameters can mimic the application of drugs that selectively block various ionic channels [e.g., tetrodotoxin is a Na^+ channel blocker (Lemon and Turner, 2000)], or the dynamic modulation of channel properties by the fish itself. While the relationships between the six parameters discussed here and the many parameters of more realistic neurons are not yet known, knowing how changes in them affect the model's behavior is still of interest (see later).

- A mimics the size of the current flowing from dendrite to soma, and thus the size of the DAP and how much it contributes towards moving the soma to spike threshold. Thus increasing A will make the neuron more likely to burst.
- r is irrelevant during periodic firing [note that (9) is independent of r], so changing it cannot switch the neuron from periodic to bursting or vice versa.

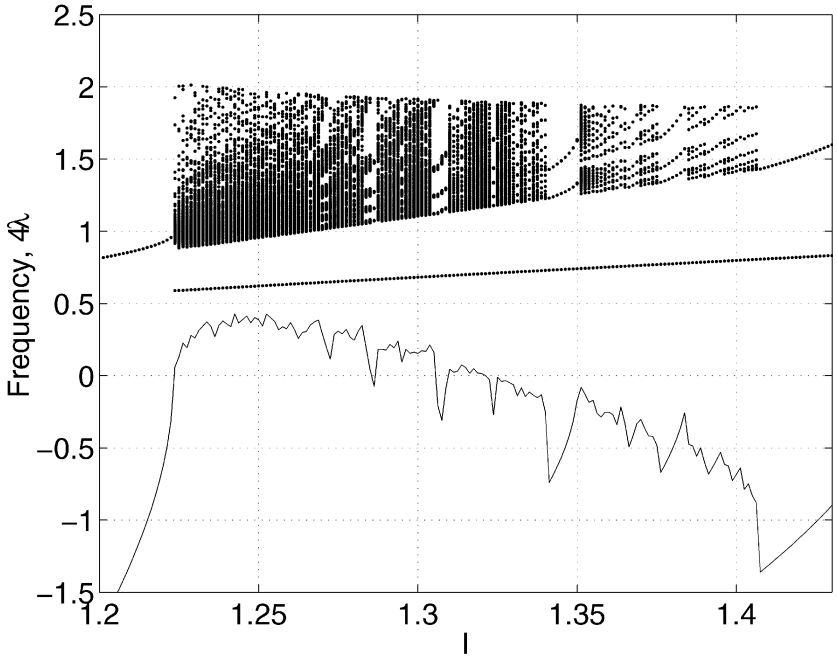

Figure 4. Instantaneous frequency and four times the most positive Lyapunov exponent (λ), as a function of input current, I, for the map (7), (8). Parameters are as in Fig. 3.

However, decreasing r makes the bursting more likely to be chaotic. This is because c can now reach a larger value at the end of a burst before it is terminated, and it is the nonlinear growth of c at the end of the burst that is the source of the chaos. However, if c can take on large values at the end of a burst, there may not be time during the interburst interval for c to decay sufficiently before the beginning of the next burst, and this can lead to an unphysical 'blow-up' in c. Note that r must be greater than σ.

- τ governs the rate of decay of c. Whether the neuron fires periodically or bursts depends on the balance between the decay of c between spikes and the increment in c at each spike. As seen from (8), increasing τ causes c to decay more slowly, making the neuron more likely to burst. Note from (1), (2) that the time-constants governing the dynamics of V and c are 1 and τ, respectively, and that it is possible for bursting to occur with $\tau < 1$ (not shown). This is in contrast to the usual analysis of bursting, where there is assumed to be a separation between the fast spiking dynamics and the slower dynamics that control the burst length and interburst intervals (Rinzel and Ermentrout, 1998; Izhikevich, 2000).

  Also, as in Doiron *et al*. (2002), there is a range of τ values for which bursting is seen as I is varied. If τ is too small, c decays too much between action potentials, and the slow growth during a burst does not occur. Similarly, if τ is too large, c cannot decay between bursts and the successive maxima of c

grow extremely quickly. This leads to 'doublet' firing in V and an eventual breakdown of the algorithm.

- For the parameters used, if $\tau > 1$, increasing σ makes the neuron more likely to burst and vice versa. If $\tau < 1$, increasing σ makes the neuron less likely to burst, and vice versa. This can be understood graphically by writing (9) as

$$e^{-\sigma} f(\Delta) = Ae^{-\sigma/\tau} g(\Delta, \tau) \tag{12}$$

where

$$f(\Delta) = I + (1 - I)e^{\Delta} \tag{13}$$

and

$$g(\Delta, \tau) = \frac{1 - e^{-\Delta/\tau} - \sqrt{1 - 2e^{-\Delta/\tau} + (1 - 4BC)e^{-2\Delta/\tau}}}{2Ce^{-2\Delta/\tau}}. \tag{14}$$

For a given τ and other parameters in the appropriate range, $f(\Delta)$ is a concave-down function of Δ, and $g(\Delta, \tau)$ is a concave-up function of Δ. They are both positive in the region of interest. The intersections of the left and right sides of (12) give the values of Δ at the two periodic orbits (one stable and the other unstable) of (1), (2). It is the coalescence of these in a saddle–node bifurcation that marks the transition from periodic to bursting behavior.

If $\tau > 1$, increasing σ decreases the left-hand side of (12) more than it decreases the right-hand side, bringing the two points of intersection closer to one another, and thus lowering the value of I at which the saddle–node bifurcation occurs. Conversely, if $\tau < 1$, increasing σ decreases the right-hand side of (12) more than it decreases the left-hand side, moving the two points of intersection further apart and thus increasing the value of I at which the saddle–node bifurcation occurs.

- B and C both control the increment in c at each spike, so increasing either will make the neuron more likely to burst. The Cc^2 term is not strictly necessary to obtain bursts, as we can produce a plot like Fig. 3 with $C = 0$ (although the bursts are then periodic, not chaotic). However, without this nonlinear term it is difficult to obtain chaotic bursts. This is because it is the nonlinear growth of c at the end of a burst, and the fact that the largest value of c during a burst is carried over to the start of the next burst, that cause chaotic dynamics to occur. If $B = 0$ then $c_n = 0$ for all n is a possible solution of (8), and having a nonzero value of B prevents this.

This knowledge is useful, since if we can determine the qualitative relationship between parameters in a more realistic model of this cell [e.g., the models in Doiron *et al*. (2001a, 2002)] and the six parameters earlier, we can understand how changing the parameters in the more realistic models will change the behavior of the cell,

without having to simulate those more detailed models. To determine these relationships, one would need to know the effects of changing a particular parameter in a large model on one or more of the six parameters discussed earlier.

As an example, it was found in Doiron *et al*. (2002) that decreasing the maximum conductance of the dendritic potassium decreased the value of current injected to the soma at which the cell switched from tonic to bursting, i.e., it made the cell more likely to burst. This is easy to understand, since it is dendritic potassium that is responsible for repolarizing the dendrite, and by lessening its effect the dendritic action potential is widened, leading to a larger DAP at the soma. Thus, decreasing this conductance is equivalent to increasing A in (1), (2). By the same reasoning, decreasing the maximum conductance of the somatic potassium in the model of Doiron *et al*. (2002) is equivalent to decreasing A, making the cell less likely to burst. A similar result regarding the effects of changing the somatic-to-total area ratio (Laing *et al*., 2002a) can be explained in a similar way.

One of the parameters in actual pyramidal cells that is thought to change over time is the contribution of slow voltage-activated persistent sodium in the dendrite (Doiron *et al*., 2001b). This becomes relevant when a cell is depolarized for a long time (of the order of 1 s). Another parameter that is thought to change on a relatively fast time-scale (although still much more slowly than the time-scale of action potential production) is the maximum conductance of dendritic potassium, whose kinetics are subject to second messenger regulation (Turner, 2002). Thus, making the link between parameters in real or realistic model neurons and the six parameters of the model presented here will increase the usefulness of this model.

2.4. ***Burst excitability.*** 'Burst excitability' (Laing *et al*., 2002b) is a type of excitability analogous to 'normal' excitability (Glass and Mackey, 1988; Gutkin and Ermentrout, 1998; Rinzel and Ermentrout, 1998; Segev and Rall, 1998; Izhikevich, 2000), except that the 'event' that follows a sufficiently strong transient excitation is a burst rather than a single action potential, and the system may return to periodic firing after a burst, rather than quiescence.

The presence of a saddle–node bifurcation of fixed points of the map (7), (8) marking the transition between periodic and burst behavior implies burst excitability at this boundary (Laing *et al*., 2002b). For a value of I less than that at the bifurcation, a temporary step increase in I may induce a burst in which the firing rate is elevated from its prior value for a time greater than the duration of the increase in I. If the magnitude of the increase in I is not sufficient, or its duration is too short, a burst will not be observed. Such behavior is shown in Fig. 5. Note that the length of the burst in Fig. 5, top, (i.e., the time between the perturbation of I and the doublet marking the end of the burst) is about four times the length of the longest time constant in the system ($\tau = 1$). The recovery from the perturbation in Fig. 5, bottom, is even longer. (There is no bistability in the system, and the long period of higher firing frequency is a result of the perturbation pushing the system very close to an unstable periodic orbit.) This reinforces the idea presented in Doiron *et al*. (2002)

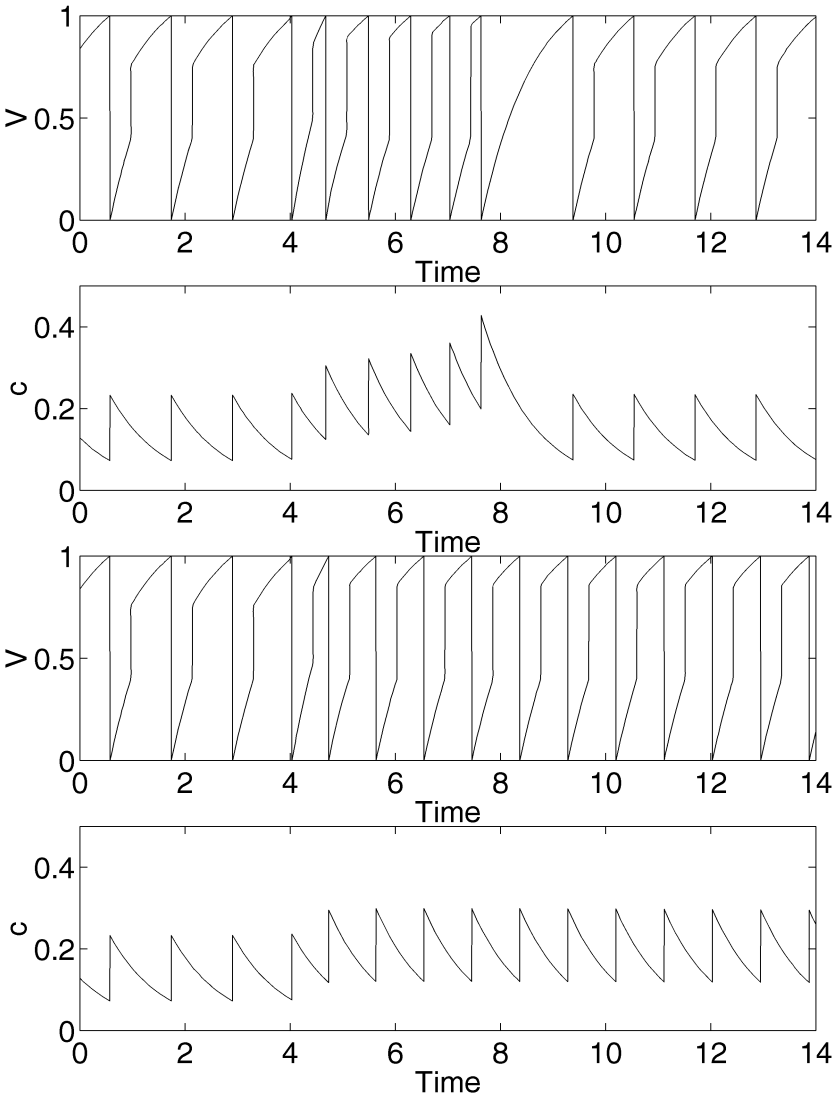

Figure 5. Burst excitability for the system (1), (2). I was set to 1.5 for $4 < t < 4.8$ for the top two panels, and 1.45 for $4 < t < 4.8$ for the bottom two panels. $I = 1.21$ otherwise. In the top two panels a burst is induced, and in the lower two no burst is induced. Note that there is no bistability in the system, and that the slow recovery after the perturbations is due to the system being pushed close to an unstable periodic orbit. Parameters are $A = 2.3$, $B = 0.15$, $C = 2$, $r = 0.6$, $\sigma = 0.4$, $\tau = 1$.

that 'slow' behavior in a bursting system does not necessarily imply the existence of a slow time-scale in the form of an explicit long time-constant, but can be the result of the system's trajectory in phase space passing close to the stable manifold of an unstable object (e.g., a fixed point or periodic orbit).

This form of burst excitability has been seen in the model presented in Doiron *et al*. (2002). Since the pyramidal cells we are modeling receive sensory input

directly from electroreceptors on the fish's skin (Nelson *et al*., 1997; Chacron *et al*., 2001), burst excitability may be a robust way of signaling a transient increase in the strength of the electric field at those electroreceptors caused by, for example, a 'chirp' emitted by another fish (Zupanc and Maler, 1993).

2.5. ***A 'gallery' of bursts.*** We know for the system (1), (2) that the current threshold for spiking is $I = 1$, and that the length of an interburst interval is given by $\Delta = \ln[I/(I-1)]$, which tends to infinity as I tends to 1 from above. Also, since the bifurcation separating periodic from bursting behavior is a saddle–node bifurcation of periodic orbits, standard results regarding type-I intermittency (Pomeau and Manneville, 1980) show that the number of spikes in a burst scales as

$$N \sim \frac{1}{\sqrt{I - I_{sn}}} \tag{15}$$

as I tends to I_{sn} from above, where I_{sn} is the value of I at which the saddle–node bifurcation occurs ($\sim$1.22 in Fig. 3). [Type-I intermittency may occur when there is a saddle–node bifurcation of periodic orbits in a system, i.e., a stable and unstable periodic orbit collide as a parameter is varied. Just after the two orbits have collided there is a 'trapping region' in phase space where the system's behavior is almost periodic. The amount of time spent in this region scales as the reciprocal of the square-root of the distance in parameter space from the bifurcation, hence the expression (15).]

The value of I_{sn} depends on the other parameters in the system, but if we can change them so that I_{sn} moves relative to the spiking threshold of 1 (and in particular, if we can make it approach 1), then we will be able to obtain a wide variety of different burst lengths and interburst intervals, as was done in Doiron *et al*. (2002). In Fig. 6 we show such a situation, where we have chosen to vary the parameter B. We can see that the curve separating periodic from burst firing touches the curve separating quiescence from periodic firing (the line $I = 1$) near $B = 0.42$. This is similar to the situation in Doiron *et al*. (2002), where the maximum conductance of dendritic potassium was varied. Note that the curve in this figure can be found numerically from (9) by determining the value of I as a function of B at which the two roots of (9) coalesce; the map, (7), (8), does not have to be iterated.

By choosing different points in Fig. 6 we can obtain different bursts—this is shown in Fig. 7. In the top panel, we are close to the curve of saddle–node bifurcations of periodic orbits, but far from $I = 1$. Hence the bursts are long (cf. those in Fig. 2) but the interburst interval is not particularly so. In the middle panel, we are close to the codimension-two point in Fig. 6 (marked with a circle), so both the bursts and the interburst intervals are long. In the bottom panel we are to the right of the codimension-two point in Fig. 6, and [as was observed in Doiron *et al*. (2002)] we observe doublets, i.e., a small ISI followed by a larger one. This is easily understood, since the first spike induces a large DAP (large because B is large) which induces a second spike. This second one marks the end of an ISI that

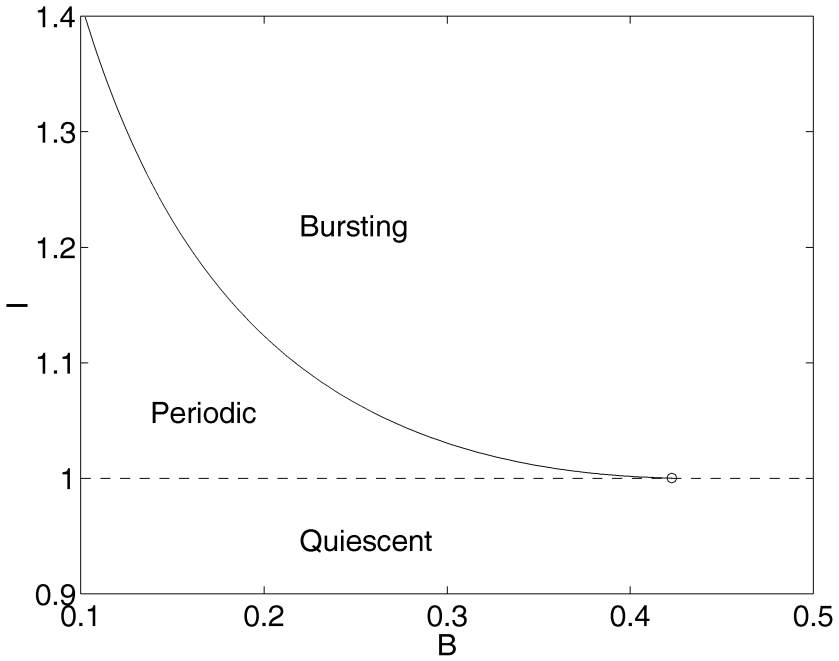

Figure 6. The curve of saddle–node bifurcations of periodic orbits (solid) and the threshold for firing (dashed), as a function of B. Other parameters are the same as in Fig. 3. The two curves meet at a codimension-two point, marked with a circle. The labels refer to the types of behavior that occur within each region of parameter space.

is within the refractory period of the dendrite, so no DAP arrives after it and a long ISI is produced (long because I is close to 1).

It is possible that the bursts produced by these cells are of most interest, rather than the individual spikes within them (Lisman, 1997). Thus being able to change both the number of spikes in a burst and the length of the interburst interval, as we have just done, may be very important with respect to changing the information content of the output of such a cell (Doiron *et al*., 2002).

One difference between the model (1), (2) and the ODE model of Doiron *et al*. (2002) involves the scaling of the interburst intervals as I decreases. The bifurcation separating quiescence from periodic firing in Doiron *et al*. (2002) is a saddle–node-on-a-circle bifurcation (Kuznetsov, 1995), and hence the period of periodic firing scales as $T \sim 1/\sqrt{I - I^*}$, where I^* is the value of the current at which the transition takes place. This is in contrast with the $\Delta = \ln[I/(I-1)]$ expression for the integrate-and-fire mechanism that we are using in (1), (2) to produce action potentials. Thus in the interburst intervals, where there is essentially no current flowing from the dendrite to the soma and the soma is driven by only the current injected into it from the outside, the length of the interburst intervals will scale differently with current for the two models. However, both scalings give the same qualitative result, i.e., $T \to \infty$ as $I \to I^*$ from above, and $\Delta \to \infty$ as $I \to 1$ from above. The scaling in (1), (2) could be made to match the scaling in

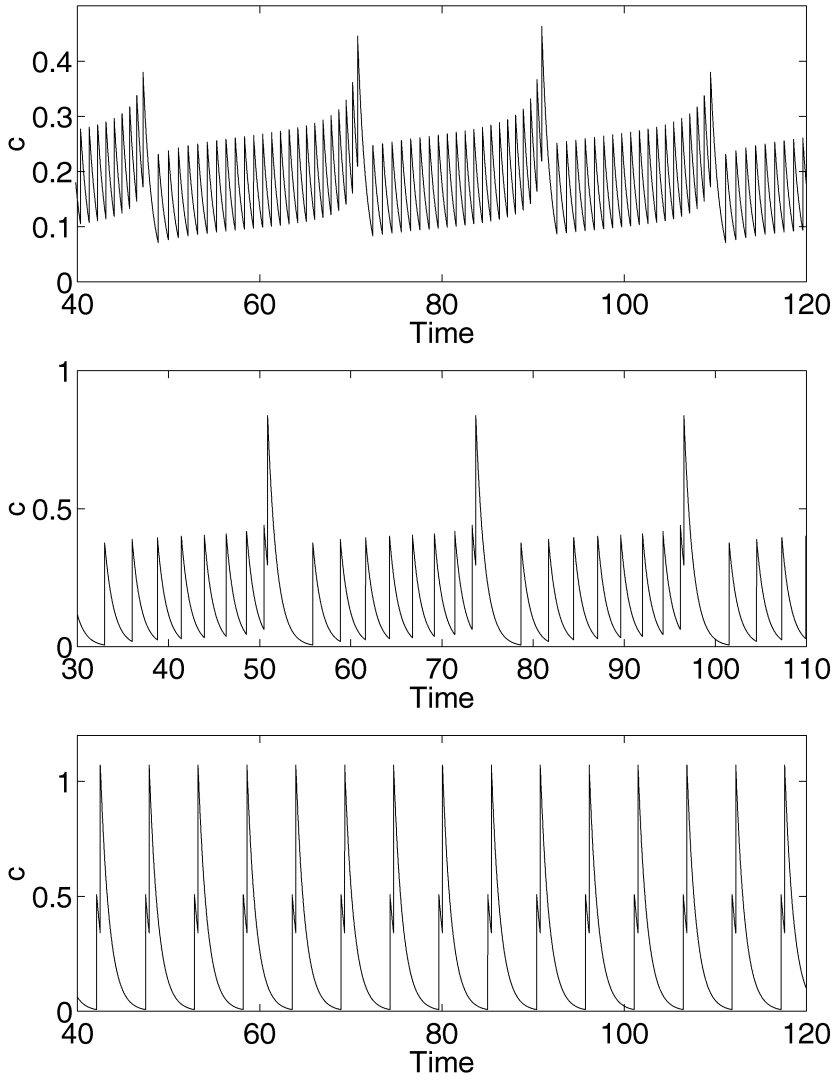

Figure 7. Example bursts of (1), (2) for three different (I, B) pairs. Top: $(I, B) = (1.23, 0.15)$, middle: $(I, B) = (1.007, 0.37)$, bottom: $(I, B) = (1.007, 0.5)$. See Fig. 6. Other parameters are the same as in Fig. 3. Note that the horizontal axes all have the same scale.

Doiron *et al*. (2002) if the spike-producing neuron was one whose bifurcation separating quiescence from periodic firing was a saddle–node-on-a-circle bifurcation; one example is the 'theta neuron' (Gutkin and Ermentrout, 1998), but its nonlinearity would complicate analysis of the resulting bursting model.

3. SINUSOIDAL FORCING

The response of dynamical systems to periodic forcing is a widely studied problem. Examples with biological motivation include Guevara *et al*. (1981); Keener

et al. (1981); Glass and Mackey (1988); Glass (1991); Coombes and Bressloff (1999); Smith *et al*. (2000); Coombes *et al*. (2001). We will now consider the situation where I in (1) is sinusoidally modulated. The modulation has amplitude Γ and angular frequency ω. This form of forcing is relevant for the following reasons. Wave-type weakly electric fish, e.g., *A. leptorhynchus*, continuously generate an approximately sinusoidal modulation of the electric field surrounding them via their electric organ discharge (EOD). The frequency of this oscillation can be as high as 1200 Hz and is essentially constant for any particular fish. Males have higher frequencies than females. When two fish are physically close, the difference in EOD frequencies gives rise to a 'beat' frequency, equal to the difference between the two EOD frequencies. Thus there are at least two types of sinusoidal inputs (the fish's own EOD and the beating oscillation) that may be detected by electroreceptors on the fish's skin (Nelson *et al*., 1997; Chacron *et al*., 2001) and passed to the pyramidal cells that we are modeling.

We will now derive a map similar to (7), (8) for the case where I in (1) is sinusoidally modulated. Since the dynamics are no longer invariant with respect to time translation, we find that they can only be reduced to a three-dimensional map, rather than a two-dimensional one as earlier.

Assume that $t = t_n^+$, $V(t_n^+) = 0$, $c(t_n^+) = c_n$, and that $t_n - t_{n-1} > r$. V evolves under

$$\frac{dV}{dt} = I - V + \Gamma \sin(\omega t) \tag{16}$$

which has the solution

$$\begin{aligned} V(t; t_n) = I\left[1 - e^{-(t-t_n)}\right] + \left(\frac{\Gamma}{1+\omega^2}\right)\{\sin(\omega t) - \omega\cos(\omega t)\} \\ - \left(\frac{\Gamma e^{-(t-t_n)}}{1+\omega^2}\right)[\sin(\omega t_n) - \omega\cos(\omega t_n)]. \end{aligned} \tag{17}$$

Note that this satisfies $V(t_n; t_n) = 0$. At a time σ after t_n,

$$\begin{aligned} V = \overline{V} \equiv I(1 - e^{-\sigma}) + \left(\frac{\Gamma}{1+\omega^2}\right)\{\sin[\omega(t_n+\sigma)] - \omega\cos[\omega(t_n+\sigma)]\} \\ - \left(\frac{\Gamma e^{-\sigma}}{1+\omega^2}\right)[\sin(\omega t_n) - \omega\cos(\omega t_n)] \end{aligned} \tag{18}$$

and $c = c_n e^{-\sigma/\tau}$. (We assume that $V(t; t_n) < 1$ for $t_n < t \leq t_n + \sigma$.) $\overline{V}$ is now incremented by an amount $Ac_n e^{-\sigma/\tau}$. If $\overline{V} + Ac_n e^{-\sigma/\tau} > 1$, i.e., if this increment pushes V over the threshold for firing, then $t_{n+1} = t_n + \sigma$. If this is not the case,

we need to solve (16) with $V(t_n+\sigma)=\overline{V}+Ac_ne^{-\sigma/\tau}$. This has the solution

$$\begin{aligned}V(t;t_n,c_n) &= I+\left(\frac{\Gamma}{1+\omega^2}\right)[\sin(\omega t)-\omega\cos(\omega t)]\\ &\quad +e^{-(t-t_n-\sigma)}\left[\overline{V}+Ac_ne^{-\sigma/\tau}-I-\left(\frac{\Gamma}{1+\omega^2}\right)\{\sin[\omega(t_n+\sigma)]\right.\\ &\quad \left.-\omega\cos[\omega(t_n+\sigma)]\}\right] \qquad (19)\\ &= I+\left(\frac{\Gamma}{1+\omega^2}\right)[\sin(\omega t)-\omega\cos(\omega t)]\\ &\quad +e^{-(t-t_n-\sigma)}\left[Ac_ne^{-\sigma/\tau}-Ie^{-\sigma}-\left(\frac{\Gamma e^{-\sigma}}{1+\omega^2}\right)[\sin(\omega t_n)\right.\\ &\quad \left.-\omega\cos(\omega t_n)]\right] \qquad (20)\end{aligned}$$

and t_{n+1} is the smallest solution greater than t_n of

$$V(t_{n+1};t_n,c_n)=1. \qquad (21)$$

All of the above is under the assumption that $t_n-t_{n-1}>r$. If $t_n-t_{n-1}<r$, i.e., there is no current flowing from the dendrite to the soma, then from (17), t_{n+1} is the smallest solution (greater than t_n) of

$$\begin{aligned}1 &= I\left[1-e^{-(t_{n+1}-t_n)}\right]+\left(\frac{\Gamma}{1+\omega^2}\right)[\sin(\omega t_{n+1})-\omega\cos(\omega t_{n+1})]\\ &\quad -\left(\frac{\Gamma e^{-(t_{n+1}-t_n)}}{1+\omega^2}\right)[\sin(\omega t_n)-\omega\cos(\omega t_n)]. \qquad (22)\end{aligned}$$

During the time interval (t_n,t_{n+1}), c decays exponentially with time-constant τ. Thus we have a piecewise map for t_{n+1} and c_{n+1} in terms of t_n, t_{n-1} and c_n:

$$t_{n+1}=\begin{cases}t_n+\sigma & \text{if } t_n-t_{n-1}>r \text{ and } \overline{V}+Ac_ne^{-\sigma/\tau}>1\\ \min\{s>t_n : V(s;t_n,c_n)=1\} & \text{if } t_n-t_{n-1}>r \text{ and } \overline{V}+Ac_ne^{-\sigma/\tau}<1\\ \min\{s>t_n : \Lambda(s;t_n)=1\} & \text{if } t_n-t_{n-1}<r\end{cases} \qquad (23)$$

$$c_{n+1}=c_ne^{-(t_{n+1}-t_n)/\tau}+B+C\left[c_ne^{-(t_{n+1}-t_n)/\tau}\right]^2 \qquad (24)$$

where $\Lambda(s;t_n)=V(s;t_n)$ and $V(s;t_n)$ is given by (17), and $V(s;t_n,c_n)$ is given by (20).

We can write the map (23), (24) as

$$t_{n+1} = f(t_n, t_{n-1}, c_n) \tag{25}$$

$$c_{n+1} = g(t_{n+1}, t_n, c_n) = g(f(t_n, t_{n-1}, c_n), t_n, c_n) \equiv h(t_n, t_{n-1}, c_n) \tag{26}$$

or

$$t_{n+1} = f(t_n, s_n, c_n) \tag{27}$$

$$s_{n+1} = t_n \tag{28}$$

$$c_{n+1} = h(t_n, s_n, c_n) \tag{29}$$

i.e., a map from $\mathbf{R^3}$ to $\mathbf{R^3}$, where

$$g(a, b, c) = ce^{-(a-b)/\tau} + B + C\left[ce^{-(a-b)/\tau}\right]^2 \tag{30}$$

and f is given by (23).

Note that when $\Gamma = 0$, $\min\{s > t_n : V(s; t_n, c_n) = 1\}$ has the solution

$$s = t_n + \sigma + \ln\left(\frac{Ac_n e^{-\sigma/\tau} - Ie^{-\sigma}}{1 - I}\right) \tag{31}$$

and $\min\{s > t_n : \Lambda(s; t_n) = 1\}$ has the solution $s = t_n + \ln[I/(I-1)]$, and the map (23), (24) reduces to (7), (8), which only involves time differences, as is expected from a time-translationally invariant system. The nonzero amplitude of forcing in (16) breaks this invariance. Note also that the map (27)–(29) has no fixed points, as the variables s and t denote firing times, not ISIs. The maximal Lyapunov exponent for (27)–(29) can be calculated in a similar way to that for the two-dimensional map (7), (8) (see Section 2.2).

3.1. ***Arnold tongues.*** Much work has been done on periodically forced oscillators (Guevara *et al.*, 1981; Glass and Mackey, 1988; Glass, 1991; Coombes and Bressloff, 1999), and it is well-known that an oscillator can become entrained to the frequency of the forcing. This may be of relevance for the model we are considering, since (as mentioned earlier) the pyramidal cells that we are modeling receive direct afferent input from electroreceptors on the fish's skin. This input has periodic components, and if a pyramidal cell was entrained to its inputs, it could faithfully track that frequency over some range. Periodically moving between the tonic state and a bursting state (so that, e.g., a burst always terminated at a fixed phase of the input) may also be a mechanism for robustly signaling a periodically changing input.

Regions of parameter space in which the frequency of the forcing and the frequency of the forced oscillator have a particular ratio are called 'Arnold tongues'

(Glass, 1991), and are labeled by the ratio of frequencies, e.g., 3 : 2. (For this example, the oscillator would pass through two cycles in the same time that the forcing signal took to pass through three cycles.) The system (1), (2) is capable of periodically oscillating for some values of its parameters and input, so under periodic forcing we expect it to have some features in common with periodically forced oscillators. However, the presence of the bifurcation separating periodic from burst firing in the unforced system may mean that new features appear when it is periodically forced.

Consider the case of $q:1$ locking, where we have one firing during a period of qT ($\omega = 2\pi/T$), i.e., during q forcing cycles. For this case, $c_{n+1} = c_n$, so let c^* be the smallest root of

$$c_n = c_n e^{-qT/\tau} + B + C\left[c_n e^{-qT/\tau}\right]^2. \tag{32}$$

We can see from (20) that in this periodically-locked state

$$\begin{aligned} 1 = I + \left(\frac{\Gamma}{1+\omega^2}\right)&[\sin(\omega t_{n+1}) - \omega\cos(\omega t_{n+1})] \\ &+ e^{-(t_{n+1}-t_n-\sigma)}\left[Ac^* e^{-\sigma/\tau} - Ie^{-\sigma} - \left(\frac{\Gamma e^{-\sigma}}{1+\omega^2}\right)[\sin(\omega t_n) - \omega\cos(\omega t_n)]\right]. \end{aligned} \tag{33}$$

Noting that for this locked state

$$\sin(\omega t_{n+1}) - \omega\cos(\omega t_{n+1}) = \sin(\omega t_n) - \omega\cos(\omega t_n) \tag{34}$$

and defining the firing phase in a similar way to Coombes and Bressloff (1999) as

$$\phi_n = \omega\left(t_n - T\,\mathrm{int}\left[\frac{t_n}{T}\right]\right), \qquad 0 \le \phi_n < 2\pi \tag{35}$$

where int$[x]$ is the integer part of x, we see that we can rewrite (33) as

$$1 = I + (1-e^{-qT})\left(\frac{\Gamma}{1+\omega^2}\right)[\sin\phi_n - \omega\cos\phi_n] + e^{-(qT-\sigma)}[Ac^* e^{-\sigma/\tau} - Ie^{-\sigma}] \tag{36}$$

where c^* is the smallest root of (32). Regarding ϕ_n as a variable, equation (36) typically has either zero or two roots, and if it has two, they are destroyed in a saddle–node bifurcation as a parameter is varied. These saddle–node bifurcations mark the edge of the $q:1$ tongue in parameter space, and a $q:1$ orbit can only exist within such a tongue.

Combining the two terms involving ϕ_n, equation (36) can be rewritten as

$$1 - I - e^{\sigma - qT}[Ac^* e^{-\sigma/\tau} - Ie^{-\sigma}] = (1 - e^{-qT})\left(\frac{\Gamma}{\sqrt{1+\omega^2}}\right)\sin(\phi_n - \tan^{-1}\omega). \tag{37}$$

The saddle–node bifurcations occur when

$$\phi_n = \pi/2 + \tan^{-1}\omega \qquad \text{or} \qquad \phi_n = 3\pi/2 + \tan^{-1}\omega \tag{38}$$

at which point the right-hand side of (37) is

$$\frac{\Gamma(1 - e^{-qT})}{\sqrt{1+\omega^2}} \qquad \text{or} \qquad -\frac{\Gamma(1 - e^{-qT})}{\sqrt{1+\omega^2}}, \tag{39}$$

respectively. Using this and rearranging (37) we see that the two values of I between which $q:1$ orbits exist are

$$I = \frac{1 - Ac^* e^{-\sigma/\tau} e^{\sigma - qT}}{1 - e^{-qT}} \pm \frac{\Gamma}{\sqrt{1+\omega^2}}. \tag{40}$$

As an example, in Fig. 8 we show the boundaries of the $1:1$ tongue, calculated using (40). This expression only gives the region in parameter space where such orbits exist, but says nothing about their stability. For ω less than $\sim$6.5, there always appears to be an orbit which is stable between the saddle–node bifurcations that mark the edges of the tongues, but for ω greater than $\sim$6.5, the $1:1$ orbit can lose stability through a Hopf bifurcation (dashed curve in Fig. 8). This is a Hopf bifurcation of a periodic orbit in the continuous system (1), (2) and corresponds to the creation of a 2-torus. This bifurcation is subcritical (Drazin, 1992; Kuznetsov, 1995), and one consequence of that is the bistability of the periodically-forced system, at least in some neighborhood to the left of this dashed line, as shown in Fig. 9. In this figure we show the behavior for $6.8 < \omega < 7.3$ when $I = 1.22$, i.e., a cut through the Hopf bifurcation in Fig. 8. The coexistence of at least two attractors (one of which is the $1:1$ locked orbit) for some range of ω values is clearly seen. This bistability has also been observed in the periodically forced six-dimensional model (Laing, 2002).

[To find the curve of Hopf bifurcations, $1:1$ phase-locked solutions of (27)–(29) were found by solving

$$\begin{aligned}(\phi + 2\pi)/\omega &= f(\phi/\omega, (\phi - 2\pi)/\omega, c) \qquad \text{and} \\ c &= h(\phi/\omega, (\phi - 2\pi)/\omega, c)\end{aligned} \tag{41}$$

for $\phi \in [0, 2\pi)$ (the phase of the forcing cycle at which the neuron fires) and c, where f and h are given by (27) and (29), respectively. The stability of these

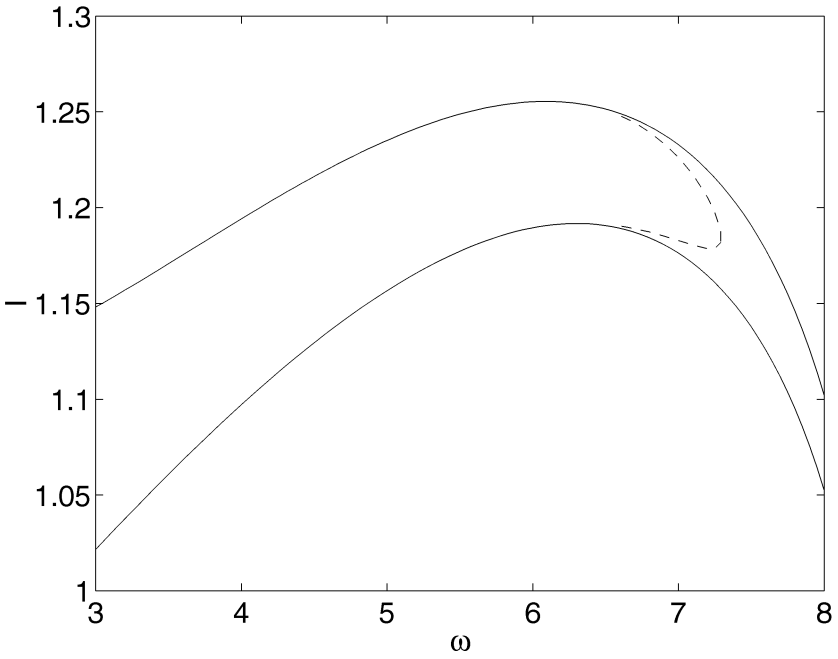

Figure 8. Boundaries of the 1 : 1 tongue from (40) (solid line) for the map (27)–(29). The dashed line indicates the curve of subcritical Hopf bifurcations. $\Gamma = 0.2$, other parameters are as in Fig. 3.

solutions was then determined by evaluating the eigenvalues of a numerically-determined approximation of the Jacobian of (27)–(29) at the corresponding points.]

This process of finding the boundaries of resonance tongues can be carried out for other frequency ratios, but the resulting equations are more complicated. Note that this procedure is not affected by the presence of the periodic $\rightarrow$ bursting boundary in parameter space. A similar observation was made in Yoshino *et al*. (1999), where the authors studied a periodically forced Fitzhugh–Nagumo system as the underlying dynamics changed from excitable to oscillatory. Note also that Fig. 8 is by no means a complete description of the dynamics, as there are an infinite number of resonance tongues in this parameter space, each labeled by the pair $p : q$, where p and q are positive integers.

Recall from Fig. 4 that when no forcing is applied, the system moves from periodic firing to bursting at $I \approx 1.22$. Referring to Fig. 8, we see that periodic forcing can *increase* the value of the DC component of the applied current at which the system starts to burst, e.g., at $\omega = 6$, as shown in Fig. 10 (top). Here, the 1 : 1 tongue straddles the value of I at which the unforced system starts to burst, and the system starts bursting at the boundary of the tongue. Conversely, sinusoidal modulation can also *decrease* the value of the DC component of the applied current at which the system moves to bursting, e.g., at $\omega = 7.15$, as shown in Fig. 10 (bottom).

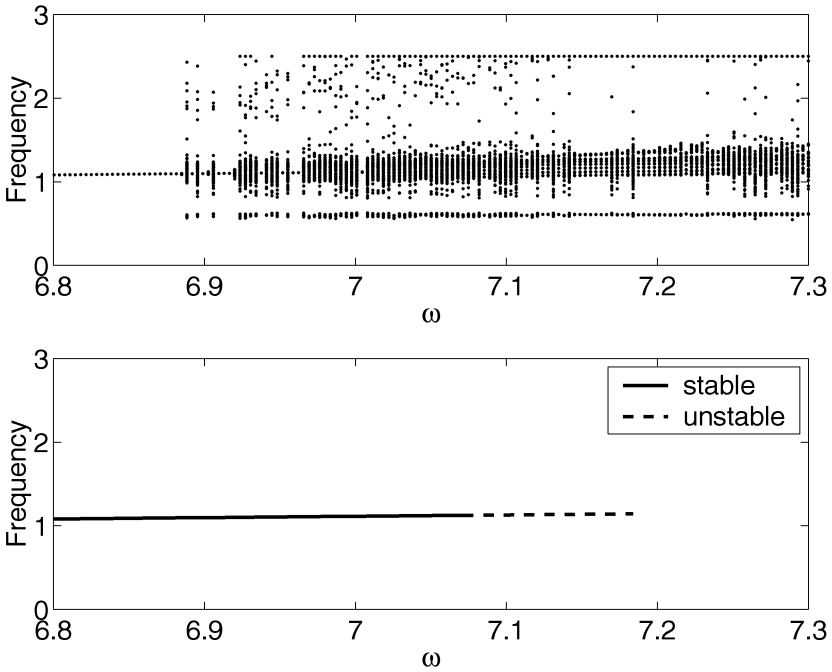

Figure 9. Bistability for the map (27)–(29) when $I = 1.22$ (cf. Fig. 8). The top panel shows iterates of the map, while the bottom one shows the 1 : 1 locked solution and its stability, for exactly the same parameter values (the 1 : 1 solution loses stability through a subcritical Hopf bifurcation—see text). Note that for $\sim 6.88 < I <\sim 7.08$, there is evidence of bistability, as the attractor in the top panel is not the same as that in the bottom panel. Parameters are as in Fig. 8.

Note that this decrease in threshold could not be predicted from looking at Fig. 8, since the transition into bursting for this value of ω does not involve leaving the 1 : 1 tongue. Thus the effective 'burst threshold' can be either increased or decreased, depending on the frequency of forcing, as was observed in Laing (2002). This phenomenon of shifting the effective threshold has not yet been observed with actual pyramidal cells, but should be straightforward to verify.

3.2. ***Stochastic resonance.*** Stochastic resonance is the phenomenon whereby moderate amounts of noise, when added to a system that has a subthreshold input signal, cause the signal to be observable in the system's output (Gammaitoni *et al.*, 1998). For small noise intensities the signal cannot be observed, as it is subthreshold, and for high intensities the system's output is swamped by the noise, so if the signal to noise ratio at the output is plotted as a function of noise intensity, it will show a maximum at some moderate value of noise intensity.

We have already derived a map, (27)–(29), for the sinusoidally forced system (1), (2), and we can use this to show stochastic resonance in (1), (2), since it already incorporates a signal—the sinusoid. One choice of modeling the effect of noise is

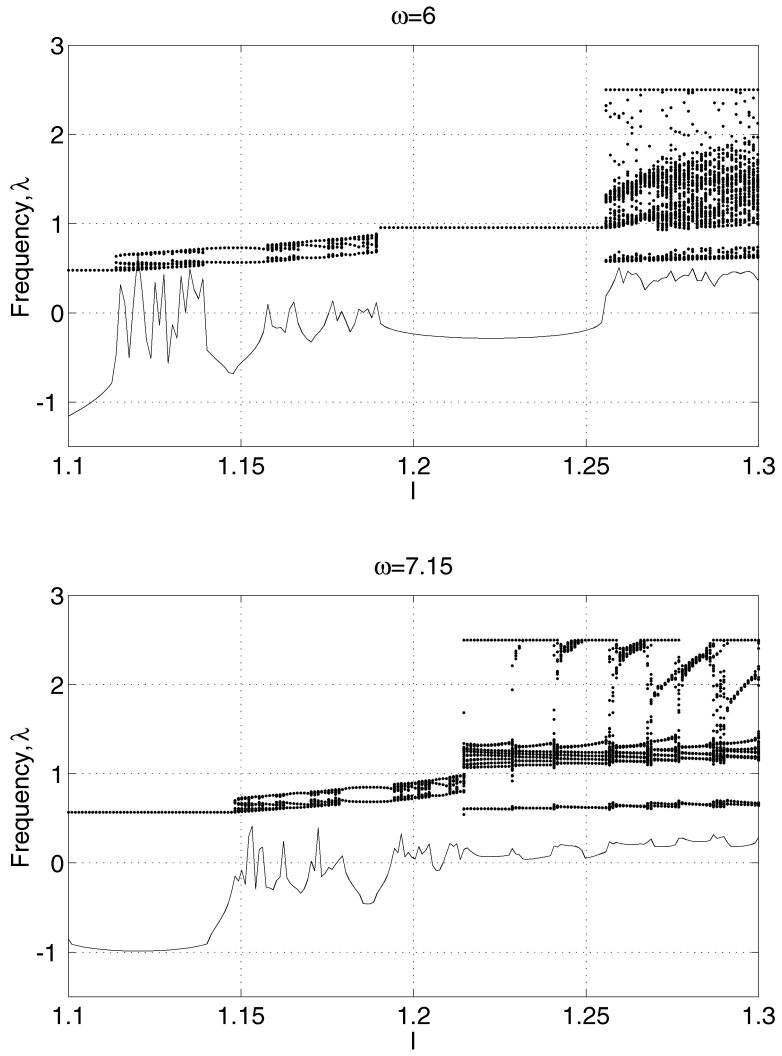

Figure 10. Instantaneous frequency (dots) and the maximal Lyapunov exponent (solid line) as a function of I for $\omega = 6$ (top) and $\omega = 7.15$ (bottom). See Fig. 8. With no periodic forcing the system shows bursts for I greater than $\sim$1.22, so depending on the frequency of forcing, periodic forcing can either increase (top) or decrease (bottom) the value of I at which the transition to bursting occurs. $\Gamma = 0.2$, other parameters are as in Fig. 3.

to replace (29) by

$$c_{n+1} = h(t_n, s_n, c_n) + \varepsilon\theta_n \tag{42}$$

where the θ_n are chosen from a normal distribution with mean zero and standard deviation 1. This noise could be due to, for example, the probabilistic nature of the opening and closing of ion channels on the neuron being modeled, or the stochastic nature of synaptic transmission from presynaptic neurons. The parameter ε controls the noise intensity.

In order to quantify the signal to noise ratio, we need to choose which aspect of the system (1), (2) is to be considered as the output. As was done in Laing (2002), we use the high-frequency 'doublets' that occur at the end of a burst. These could be detected preferentially by, for example, a synapse with facilitation that acts over a doublet ISI, but not over a typical ISI involved in periodic firing. High frequency doublets have been linked to synchronization and communication over long distances in the brain (Traub *et al*., 1996; Ermentrout and Kopell, 1998). It has also been suggested that bursts (whose presence would be signaled by a doublet, in this example) rather than spikes may be the important unit of information in neural communication (Lisman, 1997).

Thus for a set of N iterates of (27), (28) and (42) we define the output signal to be

$$f(t) = \sum_j \delta(t - \nu_j) \tag{43}$$

where

$$\{\nu_j\} = \{t_i : t_i - t_{i-1} < \rho\}_{i=2}^{N} \tag{44}$$

so $f(t)$ consists of a sum of delta functions at the times of the second spike in a pair whose ISI is less than ρ. Passing $f(t)$ through a Hanning window (Press *et al*., 1992) defined over the interval $[t_1, t_N]$ and taking the Fourier transform we have

$$F(\omega) = \frac{1}{2}\sum_j e^{i\omega\nu_j}\left[1 - \cos\left(\frac{2\pi\nu_j}{t_N - t_1}\right)\right] \tag{45}$$

and the power spectrum is $|F(\omega)|^2$. An example is shown in Fig. 11 for $\rho = 0.6$ and $N = 3000$ (the results of five realizations have been averaged). A clear increase in power at the driving frequency ($\omega = 0.1$) is seen as ε increases, but if it is increased too far, more power appears at nearby frequencies. This is quantified in Fig. 12, where we have plotted the ratio of the power at the driving frequency (0.1) to the average of the power in the range $(0.07, 0.09) \bigcup (0.11, 0.13)$. This signal to noise ratio clearly increases and then decreases as the noise intensity, ε, increases, a characteristic of stochastic resonance. This behavior is also seen if the full system, (1), (2), is simulated with Gaussian white noise added to either the dynamics of V, or the dynamics of c (not shown). Thus the noise present in this particular neural system may actually enhance the transmission of information from the fish's environment to its higher brain centers.

4. Summary and Discussion

We have presented and analyzed a two-variable delay-differential equation model for a pyramidal cell in the electrosensory lateral line lobe of a weakly electric fish. We have concentrated on the 'bursting' behavior seen in these cells. The model was

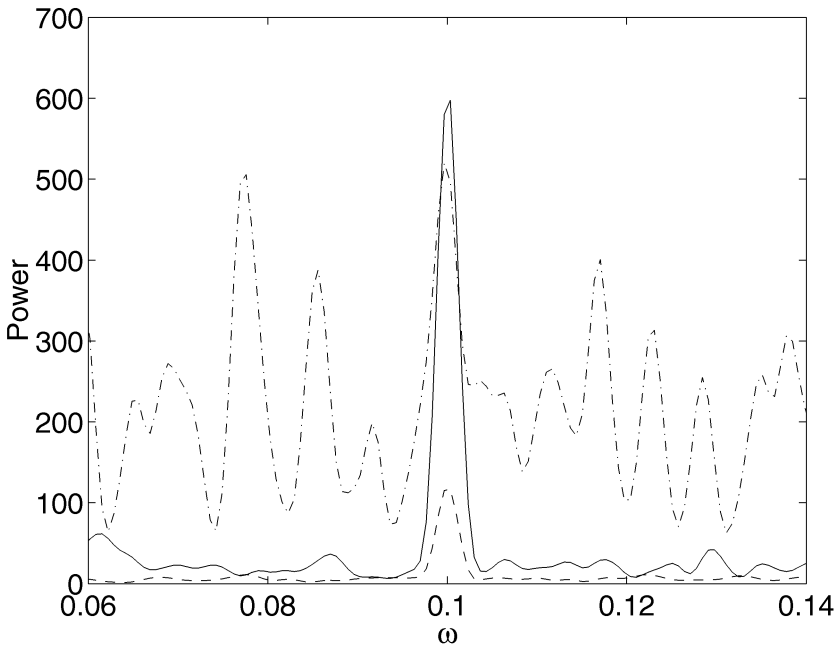

Figure 11. The power spectrum of (27), (28) and (42) as defined in (43)–(45) for $\varepsilon = e^{-6}$ (dashed), $\varepsilon = e^{-4}$ (solid) and $\varepsilon = e^{-2}$ (dash–dotted). Other parameter values are $I = 1.21$, $A = 2.3$, $B = 0.15$, $C = 2$, $\sigma = 0.4$, $\tau = 1$, $r = 0.6$, $\Gamma = 0.02$, $\omega = 0.1$. The spectra result from averaging over five noise realizations with $N = 3000$. Note that $I = 1.21$ is just below the bifurcation separating periodic from burst firing (see Fig. 3).

a simplification of the six variable ODE model presented in Doiron *et al*. (2002), which was itself a drastic simplification of the multicompartment model of Doiron *et al*. (2001a). The simplicity of our model has allowed us to derive a two-variable map for firing times of the model neuron, and to determine how the model's behavior depends on its parameters.

We have also considered the effects of sinusoidal forcing on the model neuron, and have derived a three-variable map for firing times. This map has allowed us to analytically determine the boundaries of phase-locked regions (Arnold tongues) and, by adding noise to the three-variable map, to demonstrate stochastic resonance in the model. The existence of these maps drastically decreases the computational effort of simulating the model neuron presented here, which is in turn easier to simulate than the larger models of Doiron *et al*. (2001a, 2002).

The cell we have modeled is of interest for several reasons. It receives sensory input directly from electroreceptors, and its output spike patterns are thought to encode most, if not all, of the information received by the fish about its environment. The threshold between tonic and burst firing as the input current is increased, and the variety of burst patterns produced (see Section 2.5), may both be utilized by the fish in processing this information before it is sent to higher brain regions.

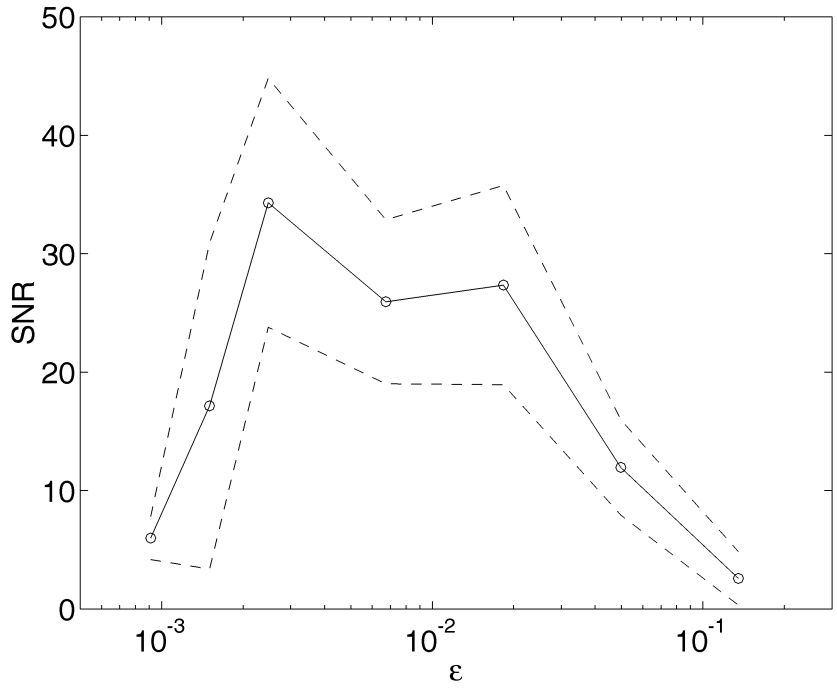

Figure 12. The signal to noise ratio of (27), (28) and (42) as defined in (43)–(45) as a function of ε. Parameters are as in Fig. 11. The dashed lines indicate $\pm$ one standard deviation.

This reduced model is of use because of its simplicity. Computationally it is much simpler to simulate than ionic models, and it also has fewer parameters that can be varied. Because of our understanding of the mechanisms we are modeling (Doiron *et al*., 2001a, 2002) we have been able to preserve the essential features of bursting in the model presented here. Once the effects of changing physical parameters in more realistic models (or actual cells) are related to the effects of changing the parameters in the model presented here, this model could be used in other investigations, for example, simulating networks of such neurons. The modeling of backpropagation in active dendrites by a delay is also novel, and may be useful in modeling other systems in which backpropagation in active dendrites (Segev and Rall, 1998; Häusser *et al*., 2000; Vetter *et al*., 2001), or the presence of a second compartment in a two-compartment model (Pinsky and Rinzel, 1994; Mainen and Sejnowski, 1996; Kepecs and Wang, 2000; Booth and Bose, 2001), is important. More generally, it may be possible to construct similar 'reduced' models of other types of bursting cells (Izhikevich, 2000). The key ingredient in the creation of (1), (2), or similar models mentioned in the appendix, is an understanding of the mechanisms involved in bursting, in particular, the effects of active backpropagation in the dendrite on the somatic action potentials.

A simple model such as the one presented here is amenable to interesting extensions. One example would be to make the refractory period of the dendrite, r,

a dynamic variable, so that it increased during a burst, as is known to occur (Turner, 2002). Then a burst could be terminated by a decreasing ISI meeting an increasing refractory period, resulting in the failure to produce a DAP. Another example could involve including a refractory period in the soma and investigating the effects of changing the refractory periods in the two compartments. Even if analytical expressions could not be obtained under these modifications, the computational simplicity of the model presented here would enable one to gain insight into their effects. It would be much harder to perform these manipulations in an ionic model for which refractory periods are not directly accessible parameters. These ideas are currently under investigation (Noonan *et al*., 2002).

Other similar work to that presented here includes (Coombes *et al*., 2001), which involves the analysis of periodic forcing of an integrate-and-fire-or-burst model neuron. The model was first presented in Smith *et al*. (2000) and, like ours, is piecewise linear. It consists of a standard integrate-and-fire model with the addition of a second variable meant to represent inactivation of a low-threshold Ca^{2+} conductance. The inclusion of this extra variable means that the model is capable of postinhibitory rebound bursting. Rulkov (2000) recently introduced a two-variable map that produced square-wave bursting, but for that map, iterates sweep out 'spikes', and do not correspond to spike times. Also, it was not derived from a continuous-time system. Goldbeter (1996) has discussed piecewise linear maps that show bursting behavior—these are approximations to Poincare maps derived from continuous-time systems. None of these models involved soma–dendrite interactions, so our model is novel in that respect.

APPENDIX: OTHER MODELS

The system (1), (2) is not unique in reproducing the qualitative features of ghost-bursting. Since we understand the mechanism involved, we can create equally valid models, each of which has its own advantages and disadvantages. This is an important point, since it implies that both the phenomenon under investigation (ghostbursting), and the model we have presented of it, are *robust* with respect to small changes in their underlying dynamics.

One equation that could replace (1) is

$$\frac{dV}{dt} = I - V + Ac \sum_n H(t_n - t_{n-1} - r) H(t - t_n - \sigma) e^{-\mu(t-t_n-\sigma)}. \qquad \text{(A.1)}$$

Here we have replaced the delayed delta function in (1), $\delta(t-t_n-\sigma)$, by a decaying exponential that is zero before $t - t_n - \sigma$, namely $H(t - t_n - \sigma)e^{-\mu(t-t_n-\sigma)}$. For this form of delayed feedback, V would be continuous at $t - t_n - \sigma$, although its first derivative would not (V would still be discontinuous at firing times). Another

alternative to (1) is

$$\frac{dV}{dt} = I - V + Ac \sum_n H(t_n - t_{n-1} - r)s(t - t_n) \tag{A.2}$$

where

$$s(t) = \frac{ab}{b-a} H(t)(e^{-at} - e^{-bt}), \qquad 0 < a < b \tag{A.3}$$

and the contribution to the term involving s from firings other than the most recent may or may not be taken into account. For (A.2), (A.3), V and its first derivative will be continuous between firings, and the time to the peak of s can be related to the effective delay between a somatic action potential and the maximum flow of current from dendrite to soma. A disadvantage of using these smoother forms of delayed feedback is that even in the unforced case, the map (7), (8) can no longer be written explicitly, but will involve equations that must be solved numerically.

It is also possible to replace the Heaviside function, $H(x)$, that determines whether there is effective feedback from the dendrite to soma in (1) with a smooth approximation, e.g., $[1 + \tanh(\nu x)]/2$, where ν is sufficiently large. Doing this would remove the distinction between cases (ii) and (iii) in (7). The $B + Cc^2$ term in (2) could also be replaced by an increasing function of c, but this would affect both the analytical tractability of the system and its chaotic nature.

It is also possible to have partial failure of backpropagation, rather than complete. This would involve replacing the Heaviside function in (1) with, for example

$$(1 - \alpha)H(t_n - t_{n-1} - r) + \alpha H(r + t_{n-1} - t_n) \tag{A.4}$$

where α is a parameter. When $\alpha = 0$, we recover (1), but for small α there is still some residual effect of the last dendritic action potential in a burst. This may be more realistic, since the last dendritic action potential does not actually fail completely (see Fig. 1, middle panel). This modification would also decrease the 'gap' between the lowest instantaneous frequency during bursting and the next lowest [see Fig. 3 and point (ii) in Section 2.1].

We could also use the 'theta neuron' (Gutkin and Ermentrout, 1998) to produce action potentials, rather than the integrate-and-fire mechanism, replacing (1) with, for example,

$$\frac{d\theta}{dt} = 1 - \cos\theta + (1 + \cos\theta)[I + AcH(t_n - t_{n-1} - r)\delta(t - t_n - \sigma)] \tag{A.5}$$

where $\theta \in [0, 2\pi)$ and the $\{t_n\}$ are the times at which θ passes through π. For this model, the transition from quiescence to periodic firing occurs as I is increased through zero. Because the bifurcation from quiescence to periodic firing when $A = 0$ is a saddle–node-on-a-circle bifurcation, as it is in Doiron *et al*. (2002), this model would have the correct scaling for interburst intervals as I is decreased.

The modifications presented above may be useful for other applications of the model (1), (2), for example, simulating an array of such neurons, and demonstrate that there is no single 'correct' model of ghostbursting, but rather a variety.

ACKNOWLEDGEMENTS

We thank Maurice Chacron and Brent Doiron for helpful conversations regarding the ideas presented here, and the referees for their very helpful comments. This work was funded by NSERC and a PREA award from the government of Ontario.

REFERENCES

Av-Ron, E., H. Parnas and L. A. Segel (1993). A basic biophysical model for bursting neurons. *Biol. Cybern.* **69**, 87–95.

Booth, V. and A. Bose (2001). Neural mechanisms for generating rate and temporal codes in model CA3 pyramidal cells. *J. Neurophysiol.* **85**, 2432–2445.

Chacron, M. J., A. Longtin and L. Maler (2001). Negative interspike interval correlations increase the neuronal capacity for encoding time-dependent stimuli. *J. Neurosci.* **21**, 5328–5343.

Coombes, S. and P. C. Bressloff (1999). Mode locking and Arnold tongues in integrate-and-fire neural oscillators. *Phys. Rev. E* **60**, 2086–2096.

Coombes, S., M. R. Owen and G. D. Smith (2001). Mode locking in a periodically forced integrate-and-fire-or-burst neuron model. *Phys. Rev. E* **64**, 041914.

de Vries, G. (1998). Multiple bifurcations in a polynomial model of bursting oscillations. *J. Nonlinear Sci.* **8**, 281–316.

Doiron, B., A. Longtin, R. W. Turner and L. Maler (2001a). Model of gamma frequency burst discharge generated by conditional backpropagation. *J. Neurophysiol.* **86**, 1523–1545.

Doiron, B., L. Noonan, R. W. Turner, A. Longtin and L. Maler (2001b). Shifting burst threshold with dendritic conductances, *XXXI Proc. Soc. Neurosci.*, San Diego.

Doiron, B., C. R. Laing, A. Longtin and L. Maler (2002). "Ghostbursting": a novel bursting mechanism in pyramidal cells. *J. Comput. Neurosci.* **12**, 5–25.

Drazin, P. G. (1992). *Nonlinear Systems*, Cambridge University Press.

Ermentrout, G. B. and N. Kopell (1998). Fine structure of neural spiking and synchronization in the presence of conduction delays. *Proc. Natl. Acad. Sci. USA* **95**, 1259–1264.

Gammaitoni, L., P. Hänggi, P. Jung and F. Marchesoni (1998). Stochastic resonance. *Rev. Mod. Phys.* **70**, 223–287.

Glass, L. and M. C. Mackey (1988). *From Clocks to Chaos: The Rhythms of Life*, Princeton University Press.

Glass, L. (1991). Cardiac arrhythmias and circle maps—a classical problem. *Chaos* **1**, 13–19.

Goldbeter, A. (1996). *Biochemical Oscillations and Cellular Rhythms: The Molecular Bases of Periodic and Chaotic Behaviour*, Cambridge University Press.

Guevara, M. L., L. Glass and A. Shrier (1981). Phase locking, period-doubling bifurcations, and irregular dynamics in periodically stimulated cardiac cells. *Science* **214**, 1350–1353.

Gutkin, B. S. and G. B. Ermentrout (1998). Dynamics of membrane excitability determine interspike interval variability: a link between spike generation mechanism and cortical spike train statistics. *Neural Comput.* **10**, 1047–1065.

Häusser, M., N. Spruston and G. J. Stuart (2000). Diversity and dynamics of dendritic signaling. *Science* **290**, 739–744.

Izhikevich, E. M. (2000). Neural excitability, spiking, and bursting. *Int. J. Bifn. Chaos* **10**, 1171–1266.

Johnston, D., J. C. Magee, C. M. Colbert and B. R. Christie (1996). Active properties of neuronal dendrites. *Annu. Rev. Neurosci.* **19**, 165–186.

Keener, J. P., F. C. Hoppensteadt and J. Rinzel (1981). Integrate-and-fire models of nerve membrane response to oscillatory input. *SIAM J. Appl. Math.* **41**, 503–517.

Keener, J. and J. Sneyd (1998). *Mathematical Physiology, Interdisciplinary Applied Mathematics*, Vol. 8, New York: Springer.

Kepecs, A. and X.-J. Wang (2000). Analysis of complex bursting in cortical pyramidal neuron models. *Neurocomputing* **32-33**, 181–187.

Kuznetsov, Y. A. (1995). *Elements of Applied Bifurcation Theory, Applied Mathematical Sciences*, Vol. 112, Springer.

Laing, C. R. (2002). The response of bursting neurons to sinusoidal inputs. In preparation.

Laing, C. R., B. Doiron, A. Longtin and L. Maler (2002a). Ghostbursting: the effects of dendrites on spike patterns. To appear in *Neurocomputing*.

Laing, C. R., B. Doiron, A. Longtin, L. Noonan, R. W. Turner and L. Maler (2002b). Burst excitability. Submitted to *J. Comput. Neurosci*.

Lemon, N. and R. W. Turner (2000). Conditional spike backpropagation generates burst discharge in a sensory neuron. *J. Neurophysiol.* **84**, 1519–1530.

Lisman, J. E. (1997). Bursts as units of neural information: making unreliable synapses reliable. *Trends Neurosci.* **20**, 38–43.

Mainen, Z. F. and T. J. Sejnowski (1996). Influence of dendritic structure on firing pattern in model neocortical neurons. *Nature* **382**, 363–366.

Nelson, M. E., Z. Xu and J. R. Payne (1997). Characterization and modeling of P-type electrosensory afferent responses to amplitude modulations in a wave-type electric fish. *J. Comp. Physiol. A* **181**, 532–544.

Noonan, L., B. Doiron, C. R. Laing, A. Longtin and R. W. Turner (2002). Dendritic spike repolarization generates a dynamic refractory period to control burst discharge. In preparation.

Pinsky, P. F. and J. Rinzel (1994). Intrinsic and network rhythmogenesis in a reduced Traub model for CA3 neurons. *J. Comput. Neurosci.* **1**, 39–60.

Pomeau, Y. and P. Manneville (1980). Intermittent transition to turbulence in dissipative dynamical systems. *Comm. Math. Phys.* **74**, 189–197.

Press, W. H., S. A. Teukolsky, W. T. Vetterling and B. P. Flannery (1992). *Numerical Recipes in C*, 2nd edn, Cambridge University Press.

Rinzel, J. and G. B. Ermentrout (1998). Analysis of neural excitability and oscillations, in *Methods in Neuronal Modeling: From Ions to Networks*, C. Koch and I. Segev (Eds), MIT Press.

Rulkov, N. F. (2000). Regularization of synchronized chaotic bursts. *Phys. Rev. Lett.* **86**, 183–186.

Segev, I. and W. Rall (1998). Excitable dendrites and spines: earlier theoretical insights elucidate recent direct observations. *Trends Neurosci.* **21**, 453–460.

Sivan, E., L. Segel and H. Parnas (1995). Modulated excitability: a new way to obtain bursting neurons. *Biol. Cybern.* **72**, 455–461.

Smith, G. D., C. L. Cox, S. M. Sherman and J. Rinzel (2000). Fourier analysis of sinusoidally driven thalamocortical relay neurons and a minimal integrate-and-fire-or-burst model. *J. Neurophysiol.* **83**, 588–610.

Steriade, M., I. Timofeev, N. Dürmüller and F. Grenie (1998). Dynamic properties of corticothalamic neurons and local cortical interneurons generating fast rhythmic (30–40 Hz) spike bursts. *J. Neurophysiol.* **79**, 483–490.

Strogatz, S. H. (1994). *Nonlinear Dynamics and Chaos: With Applications to Physics, Biology, Chemistry, and Engineering*, Reading: Addison-Wesley.

Terman, D. (1992). The transition from bursting to continuous spiking in excitable membrane models. *J. Nonlinear Sci.* **2**, 135–182.

Traub, R. D., M. A. Whittington, I. M. Stanford and J. G. Jefferys (1996). A mechanism for generation of long-range synchronous fast oscillations in the cortex. *Nature* **383**, 621–624.

Turner, R. W. (2002). Personal communication.

Vetter, P., A. Roth and M. Häusser (2001). Propagation of action potentials in dendrites depends on dendritic morphology. *J. Neurophysiol.* **85**, 926–937.

Wang, X.-J. (1993). Genesis of bursting oscillations in the Hindmarsh–Rose model and homoclinicity to a chaotic saddle. *Physica D* **62**, 263–274.

Wang, X.-J. (1999). Fast burst firing and short-term synaptic plasticity: a model of neocortical chattering neurons. *Neuroscience* **89**, 347–362.

Yoshino, K., T. Nomura, K. Pakdaman and S. Sato (1999). Synthetic analysis of periodically stimulated excitable and oscillatory membrane models. *Phys. Rev. E* **59**, 956–969.

Zupanc, G. K. H. and L. Maler (1993). Evoked chirping in the weakly electric fish (*Apteronotus leptorhynchus*): a quantitative biophysical analysis. *Can. J. Zool.* **71**, 2301–2310.

Received 18 November 2001 and accepted 15 April 2002